Modulation of the *cis*- and *trans*-Conformations in the Bis-*o*-carborane Substituted Benzodithiophenes and Emission Enhancement Effect on Luminescent Efficiency by Solidification

Kenta Nishino[1], Kyoya Uemura[1], Kazuo Tanaka[1]*, Yasuhiro Morisaki[1,2], and Yoshiki Chujo[1]*

[1]*Department of Polymer Chemistry, Graduate School of Engineering, Kyoto University, Katsura, Nishikyo-ku, Kyoto 615-8510, Japan*

[2]*Present address: Department of Applied Chemistry for Environment, School of Science and Technology, Kwansei Gakuin University, 2-1 Gakuen, Sanda, Hyogo 669-1337, Japan*

E-mail: tanaka@poly.synchem.kyoto-u.ac.jp; chujo@poly.synchem.kyoto-u.ac.jp

Keywords: carborane; aggregation-induced emission; solid-state luminescence

Abstract

Bis-carborane-substituted benzo[1,2-*b*:4,5-*b'*]dithiophenes **DCB-R** (R = H, tBu) were synthesized and characterized. Their 3-dimensional conformations were tuned by introducing the *tert*-butyl substituent at the *para*-positions of the phenyl rings. Both molecules showed emission enhancement behaviors especially in the solid state. The emission quantum efficiencies were over 0.90 in the crystalline state. Moreover, it was shown that the efficiency of **DCB-tBu** was over 0.70 in the amorphous state. From structural analyses and mechanistic investigation, it was proposed that the *tert*-butyl substituents should play a critical role in formation of the *trans*-conformation followed by suppression of aggregation-caused quenching because of the *o*-carborane units located at each plane of the benzodithiophene ring.

Introduction

Most of luminescent organic dyes suffer from critical decrease in emission efficiency by the aggregation (aggregation-caused quenching, ACQ). Even though intense luminescence can be observed in the solution state, optical properties were often spoiled via ACQ by intermolecular interaction in the solid state. One of promising platforms to overcome the ACQ problem is a class of aggregation-induced emission (AIE)-active boron complexes which show significant emission not in the diluted state but in the aggregation.[1−3] Intense solid-state luminescent properties originating from AIE were found and applied for developing the conjugated materials including polymers.[4] Additionally, based on environment-responsive intensity changes of the AIE-active materials, various types of film-type luminescent materials and sensors can be fabricated.[5−7]

It has been reported that some of the *o*-carborane[8−13] derivatives presented AIE[14−21] and can be applied as a solid-state luminescent material.[22−34] We have also focused on the aryl-modified *o*-carboranes as a scaffold for constructing luminescent "element-block",[35,36] which is defined as a minimum functional unit composed of heteroatoms.[37−40] *o*-Carborane cluster is a boron cluster composed of three-center two-electron bonds, and acts as a strong electron-withdrawing when bonding through the carbon atoms.[41−51] Thereby, bright emission from the intramolecular charge transfer (ICT) state can be generated by the combination with *o*-carborane and electron-rich aryl substituents.[52−55] Especially, even in the crystalline state, the CT emission can be often preserved by inhibiting ACQ because of the steric sphere shape of the *o*-carborane units. Thus, a variety of highly-emissive crystalline materials composed of aryl-connected *o*-

carborane structures have been obtained.[56–58] Moreover, it is known that electronic structures were drastically changed by rotation at the *o*-carborane unit.[59,60] Furthermore, it was found that these materials showed stimuli-responsive luminescent chromism toward external mechanical forces and environmental factors such as temperature.[61] However, in these materials, emission quenching often caused particularly in the amorphous state although solid-state emission via the AIE mechanism was maintained with some extent. Intermolecular interaction could severely occur at the aryl moiety in the random distribution. These unexpected emission quenching is crucially the limitation in the application of AIE-active materials to stimuli-responsive solid-state luminescent sensors by burying significant color changes. Thus, our next goal is to demonstrate preservation of the solid-state emission of AIE-active molecules from the conformation changes.

Herein, we designed bis-carborane-substituted benzo[1,2-*b*:4,5-*b'*]dithiophenes **DCB-R** (R = H, tBu). The benzodithiophene moiety in **DCB-R** would be isolated by the phenyl rings located at the adjacent position in the *o*-carborane units from intermolecular interaction in the condensed state. From the structural analyses, it was found that **DCB-H** and **DCB-tBu** formed the *cis*- and *trans*-conformations because of degree of steric hindrance at the *para*-positions of the phenyl rings, respectively. Both molecules showed emission enhancement behaviors in the solid state especially such in the crystalline state. Furthermore, it was observed that these emission intensities were maintained even in the amorphous state.

Results and Discussion

Scheme 1 shows the synthesis of **DCB-R** (R = H, ^{t}Bu). Initially, benzo[1,2-*b*:4,5-*b'*]dithiophene-4,8-dione was added to the THF solution of the lithiated ethnylbenzene derivatives **1-R**. Then, the quinone form of benzodithiophene was reduced by $SnCl_2$ in the HCl *aq*. solution, and the diethynyl derivatives **2-R** were obtained via the coupling reaction. The decaborane(14) insertion reaction was carried out to obtain the **DCB-R**. All compounds were characterized by ^{1}H, ^{11}B and ^{13}C NMR spectroscopies, elemental analyses and HRMS measurements. The products showed good stability and solubility in common organic solvents such as $CHCl_3$, CH_2Cl_2, tetrahydrofuran (THF) and benzene. Thus, we concluded that the products should have the designed structures and enough stability for performing the series of measurements.

Scheme 1

From the ^{1}H NMR spectrum of **DCB-H** in CD_2Cl_2 at 30 °C, broad signal peaks were observed, while at −30 °C, remarkable peaks were detected (Figure 1). Moreover, these spectrum changes reversibly proceeded by varying detection temperature. These data proposed that **DCB-H** can form the two types of structural isomers. These peaks were assigned by ^{1}H–^{1}H COSY (Figure S1). At −30 °C, the peaks at 8.4, 7.7, 7.1 and 6.8 ppm were assigned to the signals from the conformation A. The peaks at 7.8, 7.4, 7.2 and 7.0 ppm were attributable to those from the conformation B. Especially, the peaks at 8.4 ppm in the spectrum of the conformation A showed upfield shift to 7.8 ppm in the conformation B. The shielding effect to the benzo[1,2-*b*:4,5-*b'*]dithiophene unit could be induced by the benzene rings. Additionally, the existing ratio of the conformation A was

twice larger than that of conformation B at −30 °C, and this ratio was also changed by temperature alteration. To estimate the height of energy barrier of the isomerization, the logarithm of the existing ratio in **DCB-H** against inverse temperature was prepared (Figure S2). From this plot, thermodynamic parameters were calculated, and it was found that the conformation A was by 4.02 kJ/mol more stable than the conformation B. Because of such small energy gap, **DCB-H** formed the both conformations and showed broad peaks in the NMR spectrum in the solution at room temperature. On the other hand, **DCB-tBu** showed sharp peaks at 7.8, 7.4, 7.2, 7.0 ppm in CD_2Cl_2 at room temperature. These peaks were almost identical to the conformation B of **DCB-H**. In particular, there were no peaks around 8.5 ppm which were the specific peaks from the conformation A. These data indicate that **DCB-tBu** hardly form the conformation A-like structure. It was proposed that the steric effect of the *tert*-butyl groups could play a critical role in suppression of conformation changes.

Figure 1

To support the above speculation on the structures of these isomers, the X-ray single crystal analyses were executed. The single crystals were obtained by the recrystallization from benzene for **DCB-H** and benzene/EtOH mix solvents for **DCB-tBu**. Figures S3a−c show the ORTEP diagrams of **DCB-H**. Although probability levels were low due to thermal motions, it was observed that the benzene rings which were connected to the next carbon position in the *o*-carborane moiety were distributed to the same direction. In addition, highly symmetric structures were observed. **DCB-H** formed the *cis*-conformation in the crystal state, whereas it was clearly indicated that **DCB-tBu** had the

trans-conformation (Figures S3d−f). These facts suggest that the conformations A and B should be the *cis*- and *trans*-conformations, respectively. The structure of **DCB-tBu** should be immobilized at the *trans*-conformation because of steric hindrances of the *tert*-butyl groups. In contrast, **DCB-H** possessed the *cis*-conformation, and at −30 °C, the trans-conformation of **DCB-H** appeared. The carbon−carbon bond in the *o*-carborane unit in **DCB-H** was 1.817 Å. This bond length was much longer than that in **DCB-tBu** (1.795 Å). From the packing structure, the benzo[1,2-*b*:4,5-*b'*]dithiophene moiety showed less interaction with other benzo[1,2-*b*:4,5-*b'*]dithiophene units than the reported anthracene derivative.[61] It was implied that a smaller size of benzo[1,2-*b*:4,5-*b'*]dithiophene than that of anthracene might be responsible for suppression of intermolecular interaction in the crystal packing.

The electronic properties in the *cis*- and *trans*- conformations were calculated by using density functional theory (DFT) at the B3LYP/6-31G(d) level (Figure 2). Correspondingly, it was revealed that the *cis*-**DCB-H** had the smaller energy than *trans*-**DCB-H**, whereas the energy of *trans*-**DCB-tBu** was smaller than that of the *cis*-one. These differences should be caused by the steric effect of the *tert*-butyl groups at the *para*-position of phenyl rings. In addition, the optimized structure of *trans*-**DCB-H** seemed to involve much strain. It is implied that the π−π interaction between the one phenyl ring and benzo[1,2-*b*:4,5-*b'*]dithiophene group could be formed.

Figure 2

The UV–vis absorption spectra of **DCB-R** in THF (1.0×10^{-5} M) were measured

(Figure S4, Table S1). All samples showed the identical absorption spectra (Table 1). The absorption bands in longer wavelength region had the peaks around 400 nm. These data suggest that the substituent group at the *para* position of the phenyl ring should slightly influence on the electronic structure in the ground state. Figure 3 shows the emission properties of **DCB-R** in THF solutions and water suspensions (THF / water = 1 / 99). In the clear solution, both molecules showed the broad emission bands around 700 nm (Φ_{PL} = 0.12). The λ_{em} of **DCB-H** presented emission band with the peak at 682 nm. This value was shorter than that of **DCB-tBu** (λ_{em} = 698 nm). In contrast, the λ_{em} of **DCB-H** in the water suspension was longer than that of **DCB-tBu** (638 nm for **DCB-H** and 615 nm for **DCB-tBu**). Additionally, the Φ_{PL}s of **DCB-H** and **DCB-tBu** were 0.23 and 0.72, respectively. Hence, both molecules had aggregation-induced emission enhancement (AIEE) behaviors where emission efficiency is enhanced by solidification. By changing solvent polarity in the optical measurements, peak positions both in UV−vis absorption and emission spectra were monitored (Figure S5 and Table S2). Similarly to the ICT emission, typical peak shifts to the longer-wavelength region were observed only in the emission spectra by increasing solvent polarity, while peak shifts were hardly detected in the absorption spectra. In the plots between Stokes shifts to solvent polarity, significant slopes were found in the fitting lines from both compounds (Figure S6). These results clearly indicate that the emission bands from **DCB-R** should be originated from the ICT state. According to the previous reports, electron-accepting nature of the *o*-carborane unit play a critical role in formation of the ICT state with the electron-donating benzodithiophene moieties.[61]

Figure 3 and Table 1

Next, solid-state emission was evaluated in the crystal state. The powder samples were prepared via recrystallization from $CHCl_3$/MeOH. From the ^1H NMR and TGA measurements (Figure S7), the crystal of **DCB-tBu** involved $CHCl_3$ as a crystal solvent. $CHCl_3$ was removed by heating at 200 °C for 1 h before optical measurements. It was confirmed that any degradation and isomerization hardly proceeded in this temperature range (Figure S7). Table 1 shows the emission properties of **DCB-H** and **DCB-tBu** in the crystal in the absence of solvent molecules, aggregation and THF solutions (Figure 3). The emission spectra of **DCB-H** and **DCB-tBu** in the crystal state showed blue-shifted emission bands from those in the THF solution and water suspension (617 nm for **DCB-H** and 591 nm for **DCB-tBu**). These blue shifts could be caused by decrease of re-orientation energy.[62] The Φ_{PL} values of **DCB-H** and **DCB-tBu** were 0.90 and 0.94, respectively, and these were higher than those in the water suspension. These data clearly indicate that these molecules should have the crystallization-induced emission enhancement (CIEE) properties.[4,56–58] In the crystal packing, extension at the C−C bond in the *o*-carborane unit after excitation, which causes emission quenching in the diluted solution, should be highly restricted. Thus, it is likely that increase in emission efficiency by crystallization was induced.

In the THF solution, **DCB-H** showed emission in the shorter wavelength region than **DCB-tBu**, while solid-state emission of **DCB-H** in the water suspension and crystal was observed in the longer wavelength region. To obtain deeper insight on these behaviors, computer calculations of excited states was performed by using time-dependent density functional theory (TD-DFT) at the B3LYP/6-31G(d) level. It was confirmed that the *cis*-

conformation of **DCB-H** was also more stable than the *trans*-one in the excited state. Figure 4 presents the molecular orbitals of *cis*-**DCB-H** and *trans*-**DCB-tBu** in the excited state. Both molecules showed the σ*−π* conjugations at the C−C bond in the *o*-carborane unit. According to the previous studies, it was illustrated that the conjugated system involving the C−C bonds are the origin of the AIEE properties.[37−40] Thus, both molecules showed bright solid-state emission properties. The calculated transfer energies (corresponded transitions, wavelengths) of *cis*-**DCB-H** and *trans*-**DCB-tBu** for the emission were 1.90 eV (MO-162: LUMO → MO-161: HOMO, 653 nm) and 1.81 eV (MO-194: LUMO → MO-193: HOMO, 684 nm), respectively. These values showed good agreement with the emission spectra in the THF solution. On the other hand, in the crystalline state, the width of band gap of *trans*-**DCB-tBu** seemed to be larger than that of *cis*-**DCB-H**. In the crystal packing of **DCB-tBu**, the critical intramolecular twist was found (Figure S6). This conformational distortion is more likely to increase band gap energy. Thus, the emission band of **DCB-tBu** in the crystalline state could be detected in the shorter wavelength region although the calculation results indicated the narrower band gap from *trans*-**DCB-tBu** than *cis*-**DCB-H**.

Figure 4

Finally, emission properties in the amorphous state were evaluated. Initially, thermal decomposition and melting temperatures were determined with TGA and DSC, respectively (Figure S7). Based on these data, the amorphous state was realized by rapid cooling with the melted sample according to the powder X-ray diffraction data (Figure S8). From the ^{1}H NMR spectra, it was confirmed that less significant degradation or

isomerization were detected (Figure S7). It was found that emission from **DCB-H** was under the detectable level, meanwhile **DCB-tBu** demonstrated the almost identical spectrum to that in the water suspension around 618 nm (Table 1). It was longer than that in the crystal state. It should be emphasized that the significant high Φ_{PL} value (0.72) was obtained in the amorphous state. These data represent that **DCB-tBu** is a highly-efficient luminogen in the amorphous state.

The plausible scenario for explaining large Φ_{PL} values of **DCB-tBu** in the water suspension and amorphous state is illustrated in Figure 5. Luminescence from both molecules was obtained from the transition from the intramolecular charge transfer state in the conjugation system involving the benzodithiophene moiety as a donor and *o*-carboranes as an acceptor via the σ*−π* conjugation.[37−40] According to the ^{1}H NMR spectra, DFT-calculation and single crystal structural data, **DCB-tBu** should form the *trans*-conformation. This conformation is favorable for protecting the benzodithiophene moiety from intermolecular interaction such as π−π stacking even in the condensed state. On the other hand, since the benzodithiophene moiety was exposure in **DCB-H**, intermolecular interaction should be formed, followed by ACQ. Therefore, only **DCB-tBu** maintained high luminescence ability in the disordered solids such as amorphous.

Figure 5

Conclusion

Synthesis, structures and optical properties of dual-*o*-carborane substituted benzodithiophenes are described. The preferred structures of **DCBs** were tuned by the substituents at the *para*-positions of the phenyl rings attached to the adjacent carbon atom in the *o*-carborane units. From the synthesized molecules, AIEE and CIEE properties were demonstrated. Moreover, both molecules showed intense emission bands in the crystal state with $\Phi_{PL} > 0.90$ around 600 nm. In particular, **DCB-tBu** also showed high emission properties in the water suspension and amorphous state with $\Phi_{PL} > 0.70$ caused by the isolation from intermolecular interaction in the *trans*-conformation. The improvement of emission efficiencies in the amorphous state would be of importance in the practical usages as printed devices and bioprobes. Because of these unique optical properties in the solid state, it is suggested that both molecules could be promising "element blocks" for constructing advanced stimuli-responsive solid materials as well as for receiving AIE-active materials according to preprogrammed designs.

Experimental Section

General. All reagents such as ethynylbenzene, 4-*tert*-butylethynylbenzene, *n*-BuLi (1.6 M, hexane solution), $SnCl_2$, HCl (1.0 M, water solution), decaborane, $AgNO_3$, anhydrous toluene and acetonitrile (MeCN) were obtained from commercial sources and used without further purification. Tetrahydrofuran (THF) was purchased and purified using a two-column solid-state purification system (Glass Contour Solvent System, Joerg Meyer, Irvine, CA). ^{1}H, ^{13}C and ^{11}B NMR spectra were recorded on a JEOL JNM-EX400 instrument at 400, 100, and 128 MHz, respectively. Variable temperature ^{1}H NMR and ^{1}H-^{1}H COSY NMR spectra were recorded on a JEOL-ECS400 instrument at 400 MHz. The ^{1}H chemical shift values were expressed relative to

Me_4Si in $CDCl_3$ or CH_2Cl_2 in CD_2Cl_2 as an internal standard. The ^{13}C shift values were expressed relative to $CHCl_3$ in $CDCl_3$ or CH_2Cl_2 in CD_2Cl_2 as an internal standard. The ^{11}B chemical shift values were expressed relative to $BF_3 \cdot Et_2O$ as an external standard. High-resolution mass spectra (HRMS) were obtained on a Thermo Fisher Scientific EXACTIVE spectrometer for atmospheric pressure chemical ionization (APCI). Analytical thin-layer chromatography (TLC) was performed with silica gel 60 Merck F254 plates. Column chromatography was performed with Wakogel C-300 silica gel. UV−vis absorption spectra were obtained on a SHIMADZU UV3600 spectrophotometer. Photoluminescence (PL) spectra were obtained on a Horiba FluoroMax-4 luminescence spectrometer; absolute PL quantum efficiencies (Φ_{PL}) were determined using a Horiba FL-3018 Integrating Sphere. X-ray crystal structure analyses were performed with Rigaku R-AXIS RAPID imaging plate area detector with graphite monochromated Mo *K*α radiation (λ = 0.71069 Å) at –180 °C. The structures were solved and refined by SHELXT. X-Ray diffraction (XRD) data were obtained on a Rigaku MiniFlex diffractometer using CuKα radiation in a range of $2° \leq 2\theta \leq 50°$ at intervals of 0.01° at a scanning rate of 0.25° min^{-1}.

Synthesis

General procedure for preparing 4,8-di(arylethnyl)-benzo[1,2-*b*:4,5-*b'*]dithiophenes (2-R).

4-Ethynylaryl (3 eq.) was dissolved in THF under Ar atmosphere. Then, 1.6 M hexane solution of *n*-BuLi (3 eq.) was added to the solution at −78 °C and stirred. After 1 h, benzo[1,2-*b*,4,5-*b'*]dithiophene-4,8-dione (1 eq.) was added in one portion and stirred for 6 h at room temperature. Finally, after adding HCl solution of $SnCl_2$, colored solid was precipitated. The solid was filtered and washed with MeOH, corresponded **2-R** was obtained.

2-H: Yellow solid (41%). ^1H NMR ($CDCl_3$, 400 MHz) δ (ppm) 7.71 (d, 2H, *J* = 5.4 Hz), 7.70–

7.67 (m, 4H), 7.59 (d, 2H, J = 5.6 Hz), 7.42–7.37 (m, 6H). ^{13}C NMR ($CDCl_3$, 100 MHz) δ(ppm) 140.4, 138.3, 131.8, 128.5, 123.2, 112.0, 99.2, 85.7. HRMS (APCI) calcd. For $C_{26}H_{14}S_2$ $[M+H]^+$: 391.0610, found 391.0603. 391.0603.

2-tBu: Yellow solid (82%). ^{1}H NMR ($CDCl_3$, 400 MHz) δ(ppm) 7.71 (dd, 2H, J = 5.5, 1.4 Hz), 7.62 (dd, 4H, J = 8.4, 1.5 Hz), 7.57 (dd, 2H, J = 5.6, 1.4 Hz), 7.44 (dd, 4H, J = 8.3, 1.2 Hz), 1.36 (s, 18H). ^{13}C NMR ($CDCl_3$, 100 MHz) δ(ppm) 152.3, 140.3, 138.2, 131.6, 128.0, 125.5, 123.3, 119.9, 112.1, 99.4, 85.1, 34.9, 31.2. HRMS (APCI) calcd. For $C_{34}H_{30}S_2$ $[M+H]^+$: 503.1862, found 503.1854.

General procedure for preparing 4,8-di(2-arylcarborane-1-yl)-benzo[1,2-*b*:4,5-*b*']dithiophenes (DCB-R).

Decaborane was dissolved in MeCN under Ar atmosphere and heated at 50 °C for 1 h. After the solution turned yellow, toluene was added. Then $AgNO_3$ and **1-R** were added in one portion, and the solution was refluxed over 3 d. The black (or dark red) residue was filtered off and solution was evaporated. The crude residue was purified by silica gel column chromatography. After recrystallization by $CHCl_3$ and MeOH, **2-R** was obtained as colored crystal.

DCB-H: Orange crystal (10%).^{1}H NMR (CD_2Cl_2, 400 MHz) δ(ppm) 7.58 (s, 2H), 7.15(d, 11H), 6.87 (s,7H), 3.4–1.6 (br, 20H) ^{13}C NMR ($CDCl_3$, 100 MHz) δ(ppm) 144.2, 140.9, 131.3, 131.2, 129.9, 129.7, 128.6, 127.4, 124.1, 90.9, 64.2. ^{11}B NMR (CD_2Cl_2, 128 MHz) δ(ppm) –0.5, –0.4, –3.0, –4.2, –8.6, –9.6. HRMS (APCI) calcd. For $C_{26}H_{34}B_{20}S_2$ $[M+H]^+$: 631.4106, found 631.4105. Anal. calcd. for $C_{26}H_{34}B_{20}S_2$: C 49.82; H 5.47 found: C 46.64; H 5.35.

DCB-tBu: Orange crystal, $CHCl_3$ was contained as crystal solvent. $CHCl_3$ was removed by heating at 150 °C for 1 h, and yellow crystal was obtained. (14%). ^{1}H NMR (CD_2Cl_2, 400 MHz) δ (ppm) 7.81 (d, 2H, *J* = 6.4 Hz), 7.39 (d, 2H, *J* = 6.1 Hz), 7.18 (d, 4H, *J* = 8.6 Hz), 7.02 (d, 4H, *J* = 8.6 Hz), 3.90–1.60 (br, 20H), 1.11 (s, 18H). ^{13}C NMR (CD_2Cl_2, 100 MHz) δ (ppm) 154.5, 143.8, 141.0, 129.6, 128.4, 126.7, 126.0, 123.3, 87.1, 77.9, 34.9, 31.0. ^{11}B NMR (CD_2Cl_2, 128 MHz) δ (ppm) –1.3, –4.2, –9.0. HRMS (APCI) calcd. For $C_{34}H_{51}B_{20}S_2$ $[M+H]^+$: 743.5358, found 743.5330. Anal. calcd. for $C_{34}H_{50}S_2B_{20}$: C 55.25 ; H 6.82, found: C 55.18; H 6.70.

ACKNOWLEDGMENT

This work was partially supported by The Institute for Synthetic Organic Chemistry (for K.T.) and a Grant-in-Aid for Scientific Research on Innovative Areas “New Polymeric Materials Based on Element-Blocks (No.2401)” (JSPS KAKENHI Grant Number JP24102013).

CCDC/CSD reference numbers: DCB-H, 1583956; **DCB-tBu**, 1583957.

References

1. A. Iida, S. Yamaguchi, *Chem. Commun.* **2009**, 3002−3004.
2. A. Wakamiya, K. Mori, S. Yamaguchi, *Angew. Chem. Int. Ed.* **2007**, *46*, 4273−4276.
3. C.-H. Zhao, A. Wakamiya, Y. Inukai, S. Yamaguchi, *J. Am. Chem. Soc.* **2006**, *128*, 15934−15935.
4. K. Tanaka, Y. Chujo, *NPG Asia Mater*. **2015**, *7*, e223.
5. C. A. DeRosa, S. A. Seaman, A. S. Mathew, C. M. Gorick, Z. Fan, J. N. Demas, S. M. Peirce, C. L. Fraser, *ACS Sens*. **2016**, *1*, 1366−1373.
6. T. Butler, W. A. Morris, J. Samonica-Kosicka, C. L. Fraser, *ACS Appl. Mater. Interfaces* **2016**, *8*, 1242−1251.
7. C. A. DeRosa, M. Kolpaczynska, C. Kerr, M. L. Daly, W. A. Morris, C. L. Fraser, *ChemPlusChem* **2017**, *82*, 399−406.
8. V. I. Bregadze, *Chem. Rev.* **1992**, *92*, 209−223.
9. M. Scholz, E. Hey-Hawkins, *Chem. Rev*. **2011**, *111*, 7035−7062.
10. F. Issa, M. Kassiou, L. M. Rendina, *Chem. Rev.* **2011**, *111*, 5701−5722.
11. R. Núñez, I. Romero, F. Teixidor, C. Viñas, *Chem. Soc. Rev*. **2016**, *45*, 5147−5173.
12. R. Núñez, M. Terrés, A. Ferrer-Ugalde, F. F. d. Biani, F. Teixidor, *Chem. Rev*. **2016**, *116*, 14307−14378.
13. R. N. Grimes, *Carboranes*, 2nd ed., Academic Press, Amsterdam, 2011, 301–540.
14. R. Furue, T. Nishimoto, I. S. Park, J. Lee, T. Yasuda, *Angew. Chem. Int. Ed*. **2016**, *55*, 7171−7175.
15. S. Inagi, K. Hosoi, T. Kubo, N. Shida, T. Fuchigami, *Electrochemistry* **2013**, *81*, 368−370.

16. M. R. Son, Y.-J. Cho, S.-Y. Kim, H.-J. Son, D. W. Cho, S. O. Kang, *Phys. Chem. Chem. Phys*. **2017**, *19*, 24485−24492.

17. D. Tu, P. Leong, S. Guo, H. Yan, C. Lu, Q. Zhao, *Angew. Chem. Int. Ed*. **2017**, *56*, 11370–11374.

18. Y. Chen, J. Guo, X. Wu, D. Jia, F. Tong, *Dyes Pigments* **2018**, *148*, 180−188.

19. A. Ferrer-Ugalde, J. Cabrera-González, E. J. Juárez-Pérez, F. Teixidor, E. Pérez-Inestrosa, J. M. Montenegro, R. Sillanpää, M. Haukka, R. Núñez, *Dalton Trans*. **2017**, *46*, 2091−2104.

20. Z. Wang, T. Wang, C. Zhang, M. G. Humphrey, *Phys. Chem. Chem. Phys*. **2017**, *19*, 12928−12935.

21. X. Li, Y. Yin, H. Yan, C. Lu, *Chem. Asian J*. **2017**, *12*, 2207–2210.

22. X. Li, H. Yan, Q. Zhao, *Chem. –Eur. J*. **2016**, *22*, 1888−1898.

23. S. Mukherjee, P. Thilagar, *Chem. Commun*. **2016**, *52*, 1070−1093.

24. L. Böhling, A. Brockhinke, J. Kahlert, L. Weber, R. A. Harder, D. S. Yufit, J. A. K. Howard, J. A. H. MacBride, M. A. Fox, *Eur. J. Inorg. Chem*. **2016**, 403−412.

25. L. Weber, J. Kahlert, R. Brockhinke, L. Böhling, J. Halama, A. Brockhinke, H.-G. Stammler, B. Neumann, C. Nervi, R. A. Harder, M. A. Fox, *Dalton Trans*. **2013**, *42*, 10982−10996.

26. J. Kahlert, L. Böhling, A. Brockhinke, H.-G. Stammler, B. Neumann, L. M. Rendina, P. J. Low, L. Weber, M. A. Fox, *Dalton Trans*. **2015**, *44*, 9766−9781.

27. B. H. Choi, J. H. Lee, H. Hwang, K. M. Lee, M. H. Park, *Organometallics* **2016**, *35*, 1771−1777.

28. M. Eo, M. H. Park, T. Kim, Y. Do, M. H. Lee, *Polymer* **2013**, *54*, 6321−6328.

29. T. Kim, H. Kim, K. M. Lee, Y. S. Lee, M. H. Lee, *Inorg. Chem*. **2013**, *52*, 160−168.

30. J. J. Peterson, A. R. Davis, M. Were, E. B. Coughlin, K. R. Carter, *ACS Appl. Mater. Interfaces* **2011**, *3*, 1796−1799.

31. D. Tu, P. Leong, Z. Li, R. Hu, C. Shi, K. Y. Zhang, H. Yan, Q. Zhao, *Chem. Commun*. **2016**, *52*, 12494−12497.

32. W. Zhang, Y. Luo, Y. Xu, L. Tian, M. Li, R. He, W. Shen, *Dalton Trans*. **2015**, *44*, 18130−18137.

33. L. Zhu, X. Tang, Q. Yu, W. Lv, H. Yan, Q. Zhao, W. Huang, *Chem. Eur. J*. **2015**, *21*, 4721−4730.

34. K.-R. Wee, Y.-J. Cho, S. Jeong, S. Kwon, J.-D. Lee, I.-H. Suh, S. O. Kang, *J. Am. Chem. Soc*. **2012**, *134*, 17982−17990.

35. Y. Chujo, K. Tanaka, *Bull. Chem. Soc. Jpn.* **2015**, *88*, 633−643.

36. M. Gon, K. Tanaka, Y. Chujo, *Polym. J*. DOI:10.1038/pj.2017.56.

37. K. Tanaka, K. Nishino, S. Ito, H. Yamane, K. Suenaga, K. Hashimoto, Y. Chujo, *Faraday Discuss.* **2017**, *196*, 31−42.

38. K. Nishino, K. Hashimoto, K. Tanaka, Y. Morisaki, Y. Chujo, *Tetrahedron Lett*. **2016**, *57*, 2025−2028.

39. K. Nishino, Y. Morisaki, K. Tanaka, Y. Chujo, *New J. Chem*. **2017**, *15*, 10550−10554.

40. K. Nishino, H. Yamamoto, K. Tanaka, Y. Chujo, *Asian J. Org. Chem*. DOI: 10.1002/ajoc.201700390.

41. D. K. You, J. H. Lee, B. H. Choi, H. Hwang, M. H. Lee, K. M. Lee, M. H. Par, *Eur. J. Inorg. Chem*. **2017**, *2017*, 2496–2503.

42. L. Zhu, W. Lv, S. Liu, H. Yan, Q. Zhao, W. Huang, *Chem. Commun*. **2013**, *49*, 10638−10640.

43. J.-F. Nicoud, F. Bolze, X.-H. Sun, A. Hayek, P. Baldeck, *Inorg. Chem*. **2011**, *50*, 4272−4278.

44. M. Uebe, A. Ito, Y. Kameoka, T. Sato, K. Tanaka, *Chem. Phys. Lett*. **2015**, *633*, 190−194.

45. Y. Kameoka, M. Uebe, A. Ito, T. Sato, K. Tanaka, *Chem. Phys. Lett*. **2014**, *615*, 44−49.

46. K. Rajavelu, P. Rajakumar, M. Sudip, R. Kothandaraman, *New J. Chem*. **2016**, *40*, 10246−10258.

47. F. Teixidor, G. Barberà, A. Vaca, R. Kivekäs, R. Sillanpää, J. Oliva, C. Viñas, *J. Am. Chem. Soc.* **2005**, *127*, 10158−10159.

48. R. Núñez, P. Farràs, F. Teixidor, C. Viñas, R. Sillanpää, R. Kivekäs, *Angew. Chem. Int. Ed*. **2006**, *45*, 1270−1272.

49. F. Teixidor, R. Núñez, C. Viñas, R. Sillanpää, R. Kivekäs, *Angew. Chem. Int. Ed*. **2000**, *39*, 4290−4292.

50. A. Weller, *Nat. Chem*. **2011**, *3*, 590−596.

51. A. M. Spokoyny, C. D. Lewis, G. Teverovskiy, S. L. Buchwald, *Organometallics* **2012**, *31*, 8478−8481.

52. Y.-J. Cho, S.-Y. Kim, M. Cho, W.-S. Han, H.-J. Son, D. W. Cho, S. O. Kang, *Phys. Chem. Chem. Phys*. **2016**, *19*, 9702−9708.

53. S.-Y. Kim, Y.-J. Cho, G. F. Jin, W.-S. Han, H.-J. Son, D. W. Cho, S. O. Kang, *Phys. Chem. Chem. Phys*. **2015**, *17*, 15679−15682.

54. Z. Wang, P. Jiang, T. Wang, G. J. Moxey, M. P. Cifuentes, C. Zhang, M. G. Humphrey, *Phys. Chem. Chem. Phys*. **2016**, *18*, 15719−15726.

55. S. Kwon, K.-R. Wee, Y.-J. Cho, S. O. Kang, *Chem. Eur. J*. **2014**, *20*, 5953–5960.

56. H. Naito, K. Nishino, Y. Morisaki, K. Tanaka, Y. Chujo, *J. Mater. Chem. C* **2017**, *4*, 10047−10054.

57. K. Nishino, H. Yamamoto, K. Tanaka, Y. Chujo, *Org. Lett*. **2016**, *18*, 4064−4067.

58. H. Naito, K. Nishino, Y. Morisaki, K. Tanaka, Y. Chujo, *Chem. Asian J*. **2017**, *12*, 2134−2138.

59. L. Weber, J. Kahlert, R. Brockhinke, L. Böhling, A. Brockhinke, J.-G. Stammler, B. Neumann, R. A. Harder, M. A. Fox, *Chem. Eur. J*. **2012**, 18, 8347−8357.

60. H. Naito, K. Nishino, Y. Morisaki, K. Tanaka, Y. Chujo, *Angew. Chem. Int. Ed.* **2017**, *56*, 254−259.

61. H. Naito, Y. Morisaki, Y. Chujo, *Angew. Chem., Int. Ed.* **2015**, *54*, 5084−5087.

62. Q. Wu, T. Zhang, Q. Peng, D. Wang, Z. Shuai, *Phys. Chem. Chem. Phys.* **2014**, *16*, 5545–5552.

Figures and Tables

Scheme 1. Synthesis of **DCB-R**

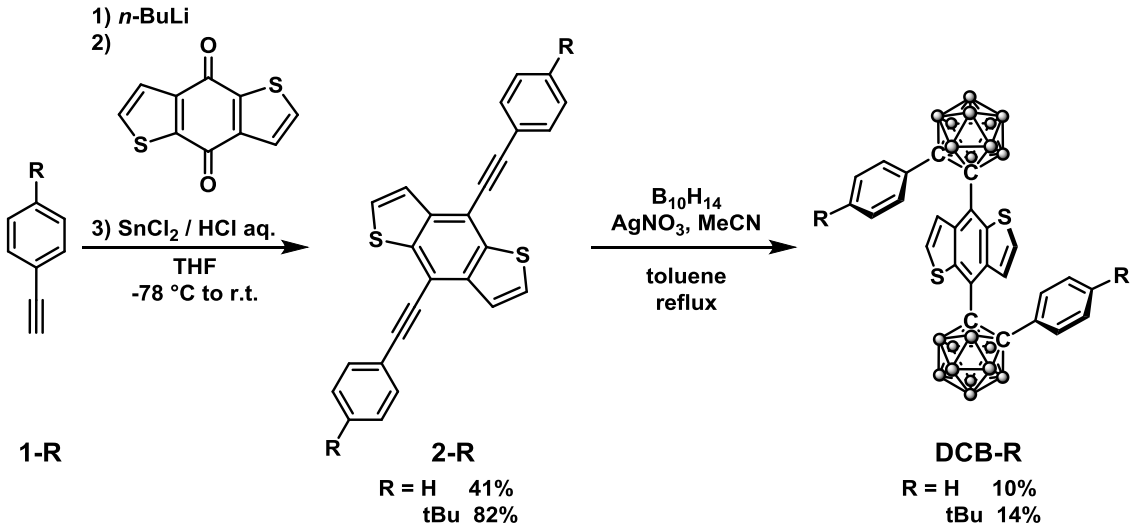

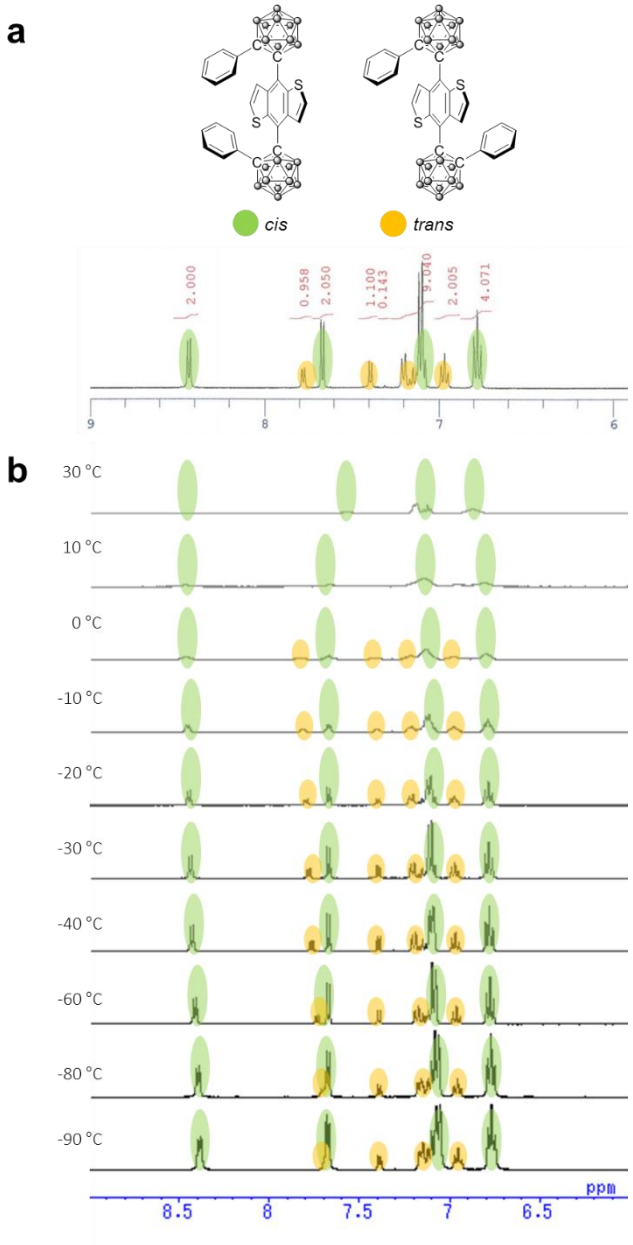

Figure 1. (a) Characterization of the ^{1}H NMR spectrum of **DCB-H** and (b) variable-temperature ^{1}H NMR spectra in CD_2Cl_2.

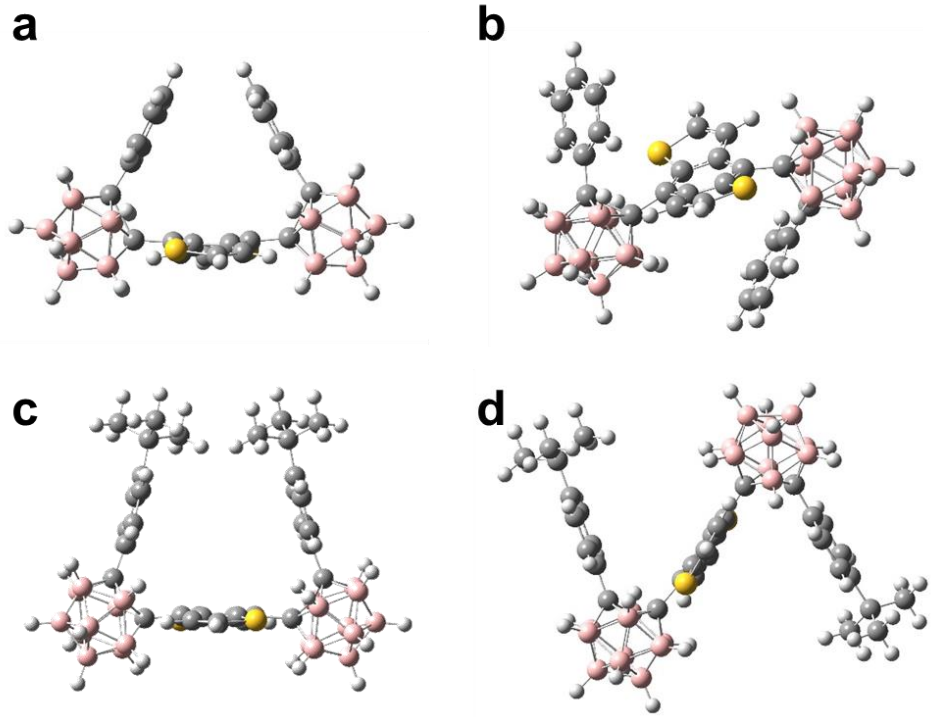

Figure 2. Optimized structures of (a) *cis*-**DCB-H**, (b) *trans*-**DCB-H**, (c) *cis*-**DCB-tBu** and (d) *trans*-**DCB-tBu** calculated at the B3LYP/6-31G(d) level.

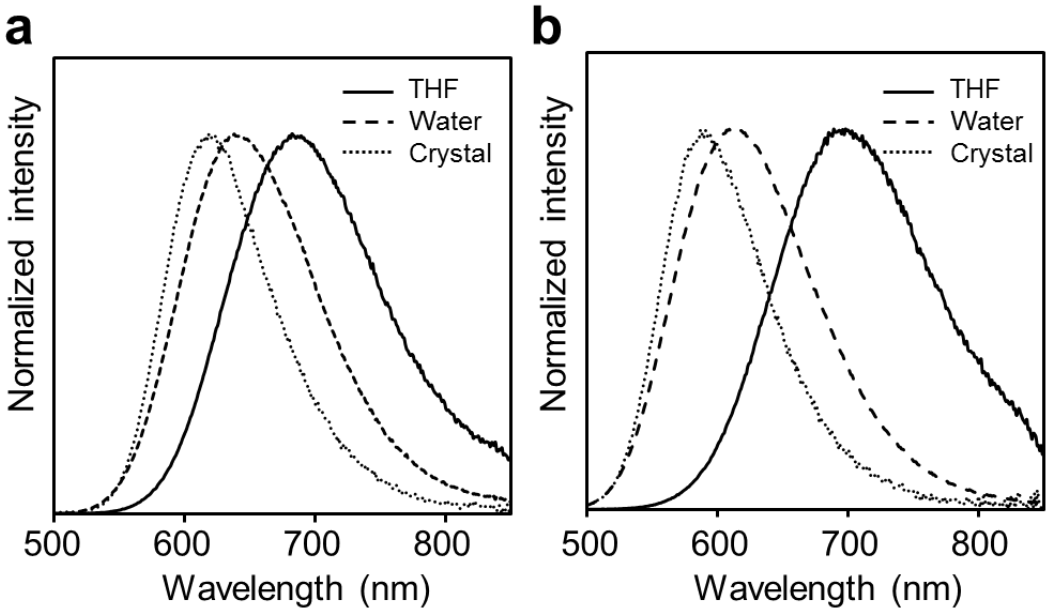

Figure 3. PL spectra of a) **DCB-H** and b) **DCB-tBu** in THF solution (solid line), aggregation (dashed line) and crystalline (dotted line) states.

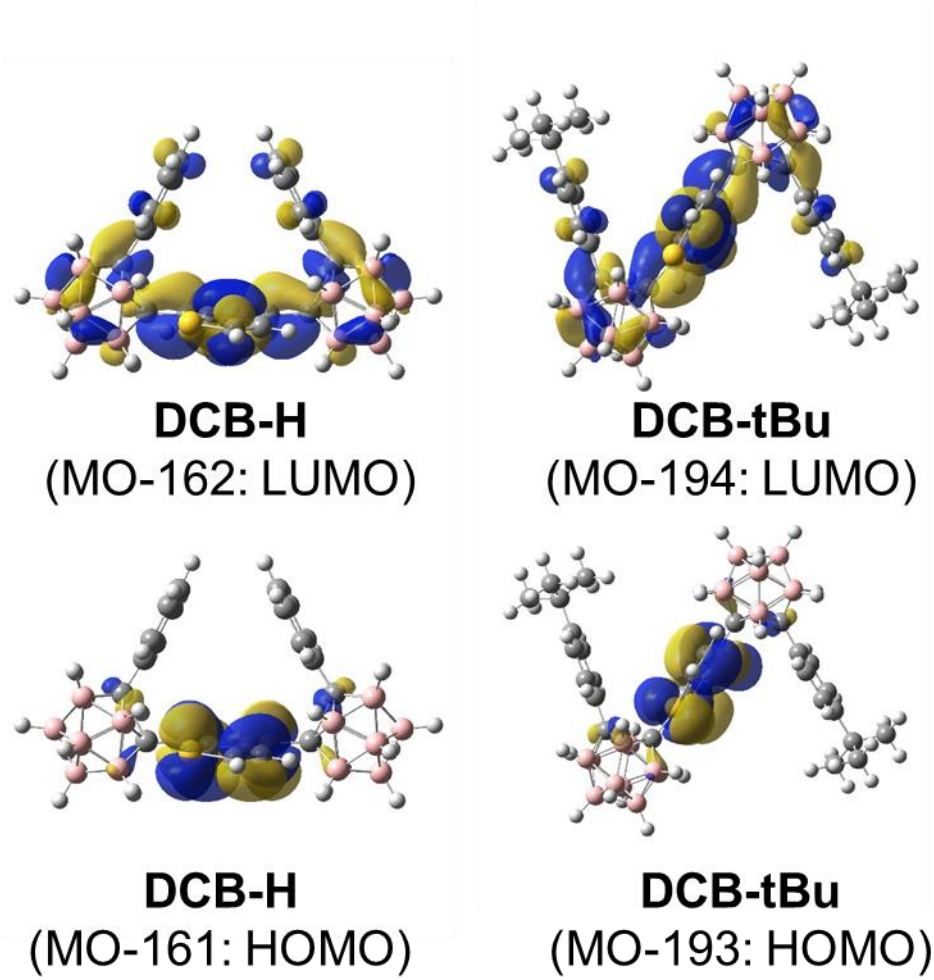

Figure 4. Calculated molecular orbitals of **DCB-R**.

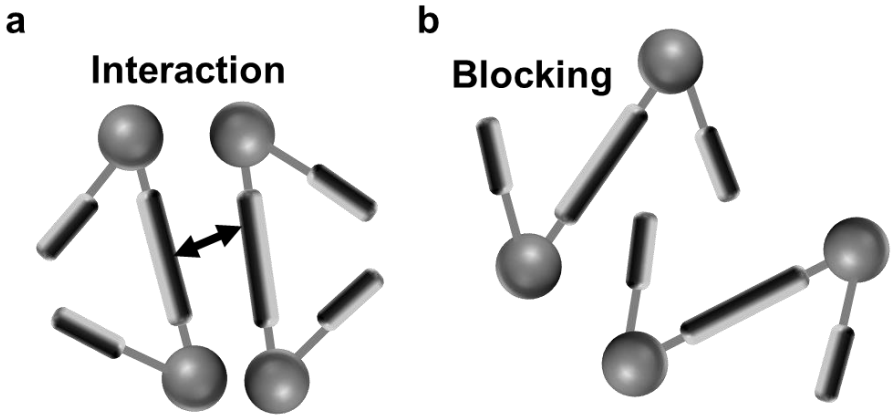

Figure 5. Schematic proposed models of intermolecular interactions in the solid samples of (a) **DCB-H** and (b) **DCB-tBu**.

Table 1. Summary of emission properties of **DCB-R**

R	THF[a]		Water		Crystal		Amorphous	
	λ_{em} (nm)	Φ_{PL}[b]	λ_{em} (nm)	Φ_{PL}[b]	λ_{em} (nm)	Φ_{PL}[b]	λ_{em} (nm)	Φ_{PL}[b]
H	682	0.12	638	0.23	617	0.90	n.d.[c]	n.d.[c]
tBu	698	0.12	615	0.72	591	0.94	618	0.71

[a] 1.0×10^{-5} M.

[b] Measured with the integrated sphere method.

[c] Not detectable due to pyrolysis.

Graphical Abstract

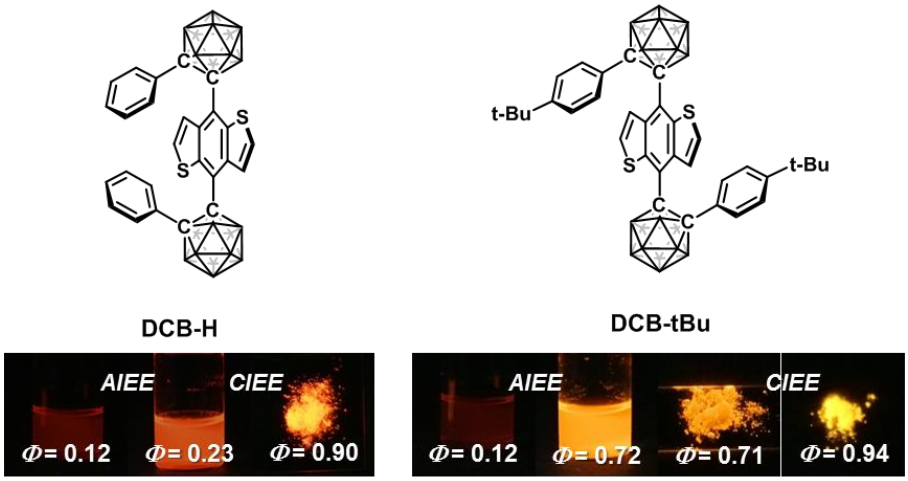

a Key Topic: Luminescent carborane

Bis-carborane-substituted benzodithiophenes with or without *tert*-butyl substituents were synthesized. It was found that their 3-dimensional conformations were tuned by introducing the *tert*-butyl substituent. Both molecules showed emission enhancement behaviors especially in the solid state.